An In Situ Creep Experiment Using a Large Rock Salt Pillar

U. Hunsche, I. Plischke, H.-K. Nipp and H. Albrecht

Bundesanstalt für Geowissenschaften und Rohstoffe
Federal Institute for Geosciences and Natural Resources (BGR)
Hannover, Federal Republic of Germany

ABSTRACT

The evaluation of constitutive laws for the creep behaviour of rock salt from laboratory experiments is an important step for the design of a radioactive waste repository in a salt dome. In addition, the validity of the results has to be confirmed for large underground rock volumes. Therefore, an in situ creep experiment was carried out by the Federal Institute for Geosciences and Natural Resources in the Asse salt mine.

A salt pillar with an edge length of 1.5 m was loaded up to 10.33 MPa with a steel flatjack, which was inserted in a horizontal slit in the middle of the pillar. The displacements were measured for several months in different directions by numerous displacement transducers. The average steady-state strain rates in the vertical and horizontal directions of the two cubed-shaped pillar halves were calculated from these measurements for stresses of 9.3 and 10.33 MPa. The influence of the experiment on the vertical convergence of the drift was measured with multi-extensometers by the Institut für Tieflagerung (IfT), Gesellschaft für Strahlen- und Umweltforschung (GSF). The experiment was supplemented by laboratory creep experiments on the same material.

The comparison of the experiments with each other and with the previously derived creep law yields a consistent picture. Only the measured horizontal strain rates are too large in relation to the vertical rates. For a refined evaluation, a finite element model calculation was carried out using a computer program (ANSALT).

From the results, it can be concluded that the steady-state creep behaviour of a large underground rock salt volume follows the same creep law as small laboratory samples.

INTRODUCTION

Within the scope of research work for the final deposition of radioactive waste in a rock salt formation, the rheological behaviour of rock salt has been intensively investigated during recent years. In the Federal Institute for Geosciences and Natural Resources (BGR), the Federal Republic of Germany (FRG), based on theoretical investigations and many experimental investigations, a law was developed for the steady-state creep of natural polycrystalline rock salt. The form of this law is based on the physical principles of deformation mechanisms, as described in many publications, e.g., Ashby (1972), Frost (1974), Langdon (1978) and Albrecht and Hunsche (1980). For conditions of up to 20 MPa and 300°C, covered during creep tests in the BGR, the deformation mechanism of dislocation climb dominates. For the creep law, the following equation is applicable:

$$\dot{\epsilon}_s = A \cdot \exp(-Q/RT) \cdot \left(\frac{\delta}{\delta^*}\right)^n$$

where

$\dot{\epsilon}_s$ = steady-state strain rate
A = structural factor
Q = activation energy
R = universal gas constant
σ = compressive stress
n = stress exponent
σ^* = 1 MPa: normalizing stress.

The values determined in the BGR from many tests for constants A, Q and n are given in Section 4. The result is described in detail and substantiated by Wallner et al. (1979), Albrecht and Hunsche (1980) and also Hunsche (1982). It is worthy of note that the creep law constants determined by Herrmann, Wawersik and Lauson (1980) for natural polycrystalline rock salt agree well with those determined in the BGR. This is a corroboration that both laws reliably reproduce the actual conditions.

Although the BGR creep law has long been used for computing the long-term stability and deformation be-

haviour of underground cavities, it has, however, not hitherto been fully clarified whether such a creep law determined on relatively small laboratory samples can be readily applied to large volumes of rock.

From strength investigations carried out on different types of rock, such a size effect is well known and, for example, described and analysed by Tsue-Lavie and Denekamp (1982). According to this, the strength is reduced in uniaxial compression tests with increasing sample size, in particular when the material shows brittle fracture. This effect was, however, not observed with the ductile failure of rock salt. According to Dreyer (1972), there is even an increase in strength in the case of small sample sizes and with an increase in size, a constant value.

Such a size effect is not known in creep tests and has also apparently not as yet been investigated.

To come closer to clarification of this problem, an in situ creep test was carried out by the BGR on a large salt pillar. In this case, an accurate knowledge of the stress in the vertical direction is of the utmost importance. As the measurement of stresses in rock salt is, however, most problematic, the required stress was developed and regulated at the centre of the pillar with the help of a large flatjack.

The most important aim of the test was to compare the measured steady-state creep rates with the forecasts from the creep law. The test has, to a great extent, been successfully concluded. The most important results are presented in this paper.

DESCRIPTION OF THE EXPERIMENT

The test site is located on the 490 m level in the Asse II salt mine of the Gesellschaft für Strahlen- und Umweltforschung (GSF) near Wolfenbüttel. Stratigraphically, it is situated in Na 3 γ (Liniensalz). The test pillar dimensions are 1.5 × 1.5 × 3.0 m. It is connected at the roof and floor with the rock. It was constructed with a road header by a GSF team. Careful cutting was given the highest priority during construction of the pillar.

The horizontal slit necessary for installation of the flatjack was constructed at the centre of the pillar, using a hole-to-hole procedure. The drill holes were made using a core drill in a dry drilling procedure. Creep tests were carried out for comparison purposes in the laboratory on the cores obtained by drilling.

The flatjack was welded together out of two square steel plates 3 mm thick with an edge length of 1.5 m, as well as four 5-mm-thick slitted tubes with an outer diameter of 80 mm, so that the tubes formed a deformable bulge around the flatjack.

The two bearing-surface areas of the flatjack were covered in each case with three 4-mm-thick hard-boards, for better distribution of pressure and to smooth out minor unevenness. After inserting the flatjack into the slit the remaining cavity was filled with a mixture of brine, salt and a special cement.

In order to be able to mount the linear variable differential transformer (LVDT) transducers and dial gauges necessary for measuring displacements to the two pillar halves, 18 measuring pins were anchored on each of the four pillar sides. The pins were sunk about 15 cm deep into the pillar sides.

The distances of the pins from one another were regularly measured, in order to have an additional method for recording displacements and consequently to be able to carry out comparisons with the measurements of the LVDT transducers and gauges.

The changes in distance between a number of measuring pins were measured with the aid of 26 (23 vertical, 3 horizontal) LVDT transducers and 6 gauges. As an example, the measuring arrangement of pillar side 4 can be seen in Figure 1.

A nitrogen gas cylinder served as the energy source for production of pressure. An adjustable reducing valve re-

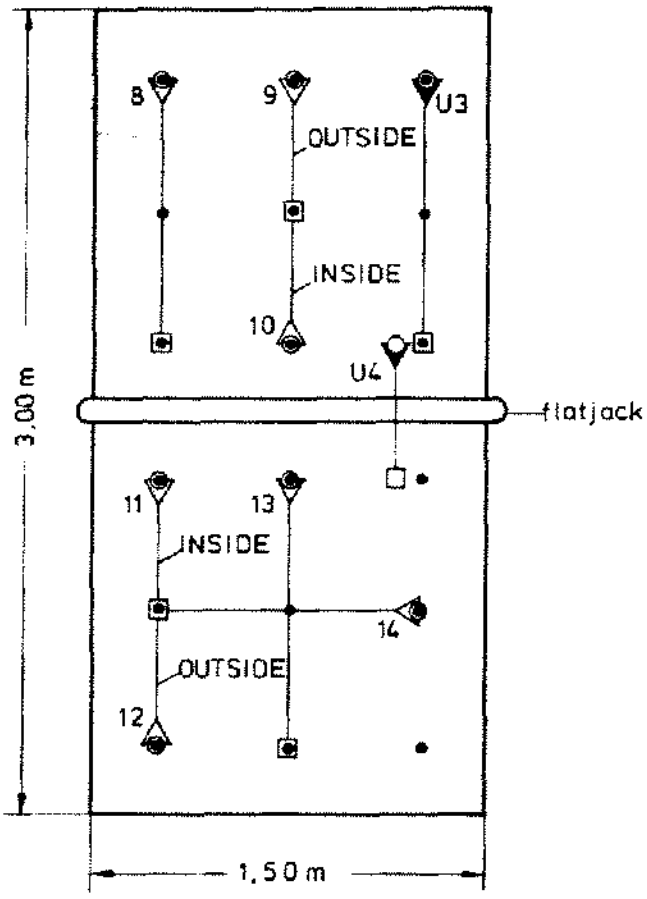

Figure 1. Arrangement of measuring intervals on side 4 of the pillar. Numbers: Measuring intervals with inductive displacement transducers. U3, U4: Measuring intervals with dial gauges. •: Measuring pins.

duced the cylinder pressure to a lower pressure, which operated a hydraulic pump that functioned as a pressure intensifier and developed the oil pressure for the flatjack, with an intensification ratio of 1 : 12 (see Figure 2).

The oil pressure contained in the flatjack was recorded by an electrical pressure gauge and displayed additionally on a manometer.

Due to the pillar and flatjack geometry, the pressure in the pillar is slightly higher than that in the flatjack: 90 bar in the flatjack corresponds to 9.3 MPa in the pillar, 100 bar produces 10.33 MPa. This correction was taken into consideration in the evaluation.

Apart from the stress, the creep behaviour of rock salt is greatly influenced by the temperature. For this reason, the temperature of the salt pillar was measured with a resistance thermometer (PT 100) that was positioned in a 30-cm-deep drill hole. Further, the ambient temperature and that of the surrounding rock were measured.

The data were collected by electronic equipment installed at the test site. They were then digitized, passed by means of a cable above ground and recorded hourly on magnetic tape. Parallel thereto the measurement data were recorded on a recorder via a digital/analog transducer. This served to give better monitoring of the test from the surface. Recording on a separate tape then followed on the GSF central computer. At the BGR the data were documented, treated statistically and evaluated.

The Institut für Tieflagerung, GSF, complemented the in situ test with convergence measurements on 8 multi-extensometers, which were anchored onto the roof and floor on each side of the pillar in 9-m-deep vertical boreholes, at a distance of 30 cm from the test pillar. The extensometer measuring points are located at depths of 0.75 m, 1 m, 3 m and 9 m in the boreholes. Conclusions concerning the deformation behaviour of the surrounding rock under the influence of the in situ test were to be drawn from these measurements. The measuring arrangement of the multi-extensometers is schematically shown in Figure 3.

In addition, two Sandia strain-gauged stress meters (SGS) from Sandia National Laboratories, U.S.A. were built into one pillar half in order to undergo a test under defined conditions in rock salt. Moreover, because the

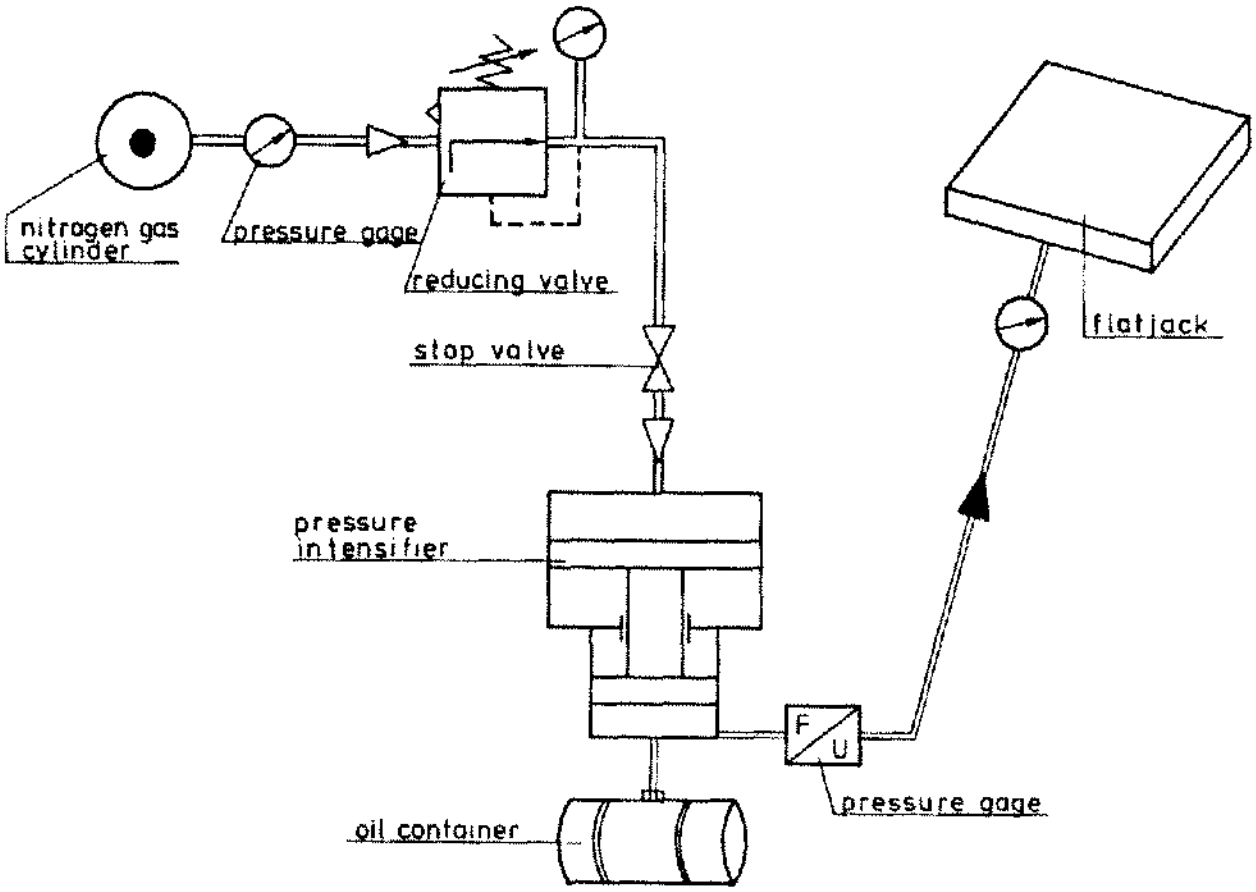

Figure 2. Schematic of the pressure unit set-up.

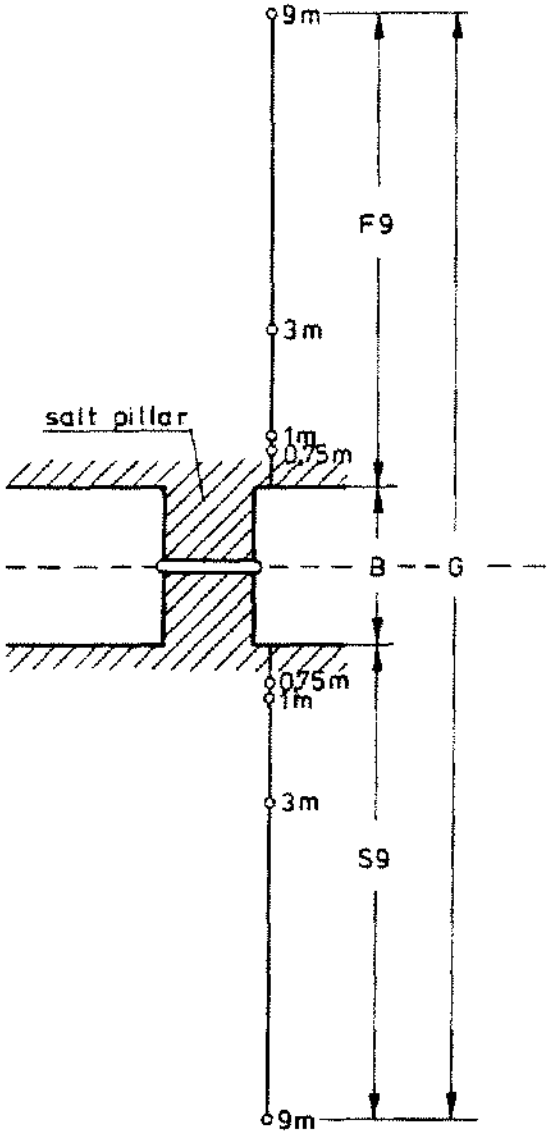

Figure 3. Arrangement of the extensometer fixed points. The deformations of measuring intervals F9, B, G and S9 are described in Section 3. Similar multi-extensometers are positioned on all four pillar sides.

stress conditions in the test pillar were known, a calibration method was thus available for these hard-inclusion stress meters.

In cooperation with the Institut für Messtechnik im Maschinenbau, University of Hannover, two coherent optical measuring methods were tested for the first time below ground on the test pillar (holography and speckle technique) for measuring deformation. These methods are different from conventional measuring techniques in that they work on a no-contact basis; the measurements are made for an entire area simultaneously for all surface points. For each measured point, the two- or three-dimensional deformation vector can be very accurately measured later using a photo plate. The results obtained with this method will be published separately.

The test was started on 5 Oct. 1981. By raising the pressure in a stepwise progression, a flatjack pressure of 90 bar was achieved on 19 Oct. 1981 and held constant. On 18 Jan. 1982 the pressure was raised to 100 bar and again held constant. On 23 March 1982 the control device was switched off and the flatjack was sealed off. In this way the stress produced in the pillar by the rock load was to be measured. The chronological development of pressure in the pillar is shown in Figure 4.

The results given in the following are related to the period up to 23 March 1982 and contain two relatively long phases with 90 and 100 bar flatjack pressure, during which the creep behaviour of the salt pillar was observed. The measured pressure varies at a maximum ± 3 bar from the set pressure. Thereafter, several stress variation tests were also carried out, which are reported on elsewhere. At the present, the test is once again in a phase of constant load.

MEASUREMENT RESULTS

The temperature of the salt pillar and the oil pressure in the flatjack are recorded as test parameters. The most important measurement results are the continuous displacement measurements in the vertical direction. The deformations and strain rates determined from these data were drawn on for comparison with the creep law determined in the laboratory. In addition, the horizontal displacements were also measured over three sections. The results are required for a refined evaluation and for model calculations.

Throughout the whole test the temperature of the salt pillar was 28.5°C $\pm$ 0.3°C.

From the measured pressures, vertical stresses of 9.3 and 10.33 MPa were obtained for the two creep phases in the pillar evaluated here. Maximum variations amounted to $\pm 3\%$.

As an example for the deformation measurements, the deformation-time curves of some vertical measurement sections and the three horizontal measurement sections, up till 20 May 1982, are shown in Figures 5–7. It can be seen in all the curves that the load was increased stepwise to 9.3 MPa and that steady-state creep was achieved after a phase of transitional creep. After the load increase to 10.33 MPa on 18 Jan. 1982, transitional creep and steady-state creep are again observable in the curves. Sealing off the flatjack on 23 March 1982 is noticeable as a distinct bend in the deformation curves.

There are some characteristic differences in the deformation of the individual pillar sides and pillar halves. Therefore, to solve the problem posed in this paper, mean values of the displacements or the strain rates were always calculated for all four pillar sides.

In order to give an impression of the mean deformations

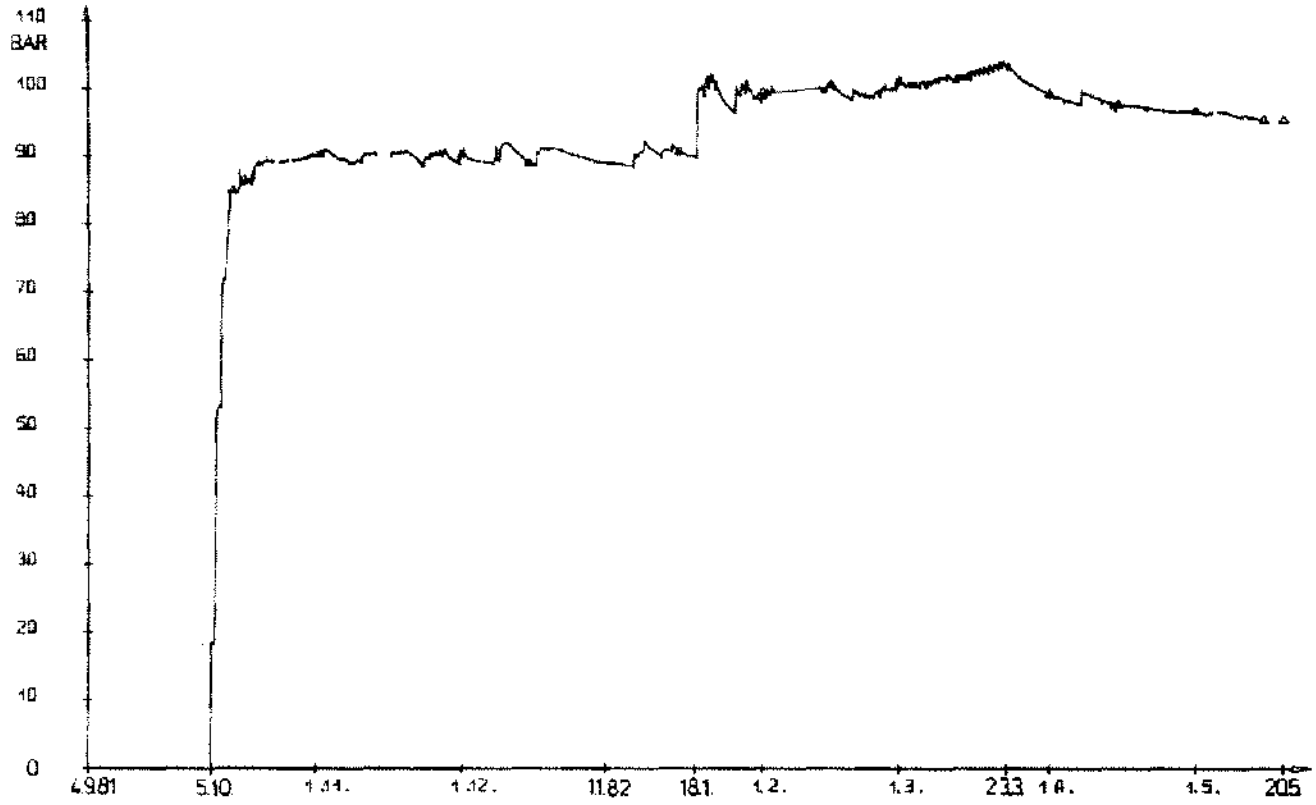

Figure 4. Chronological development of pressure in the flatjack. The time axis begins with construction of the slit.

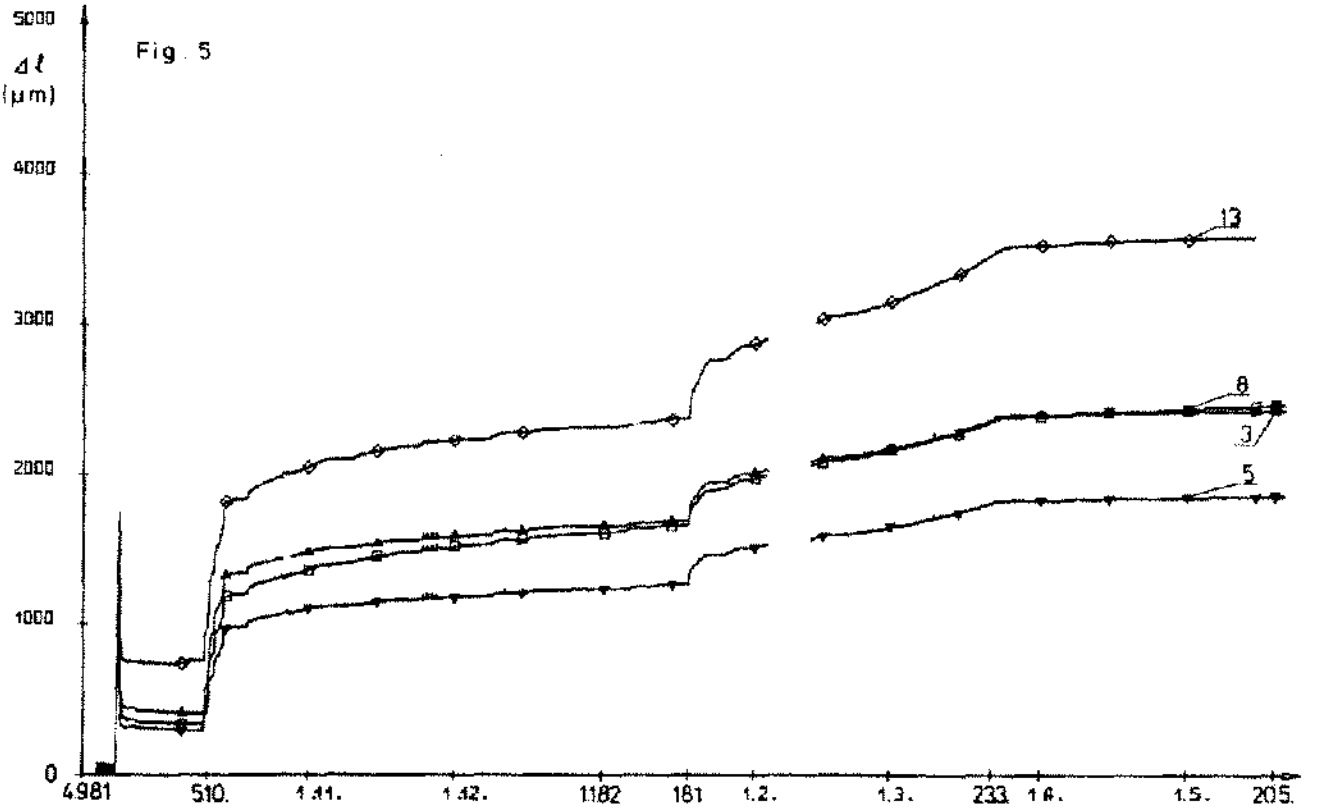

Figure 5. Deformation-time curves of four vertical measuring intervals. Measuring interval 1 m. Numbers indicate numbers of measuring intervals.

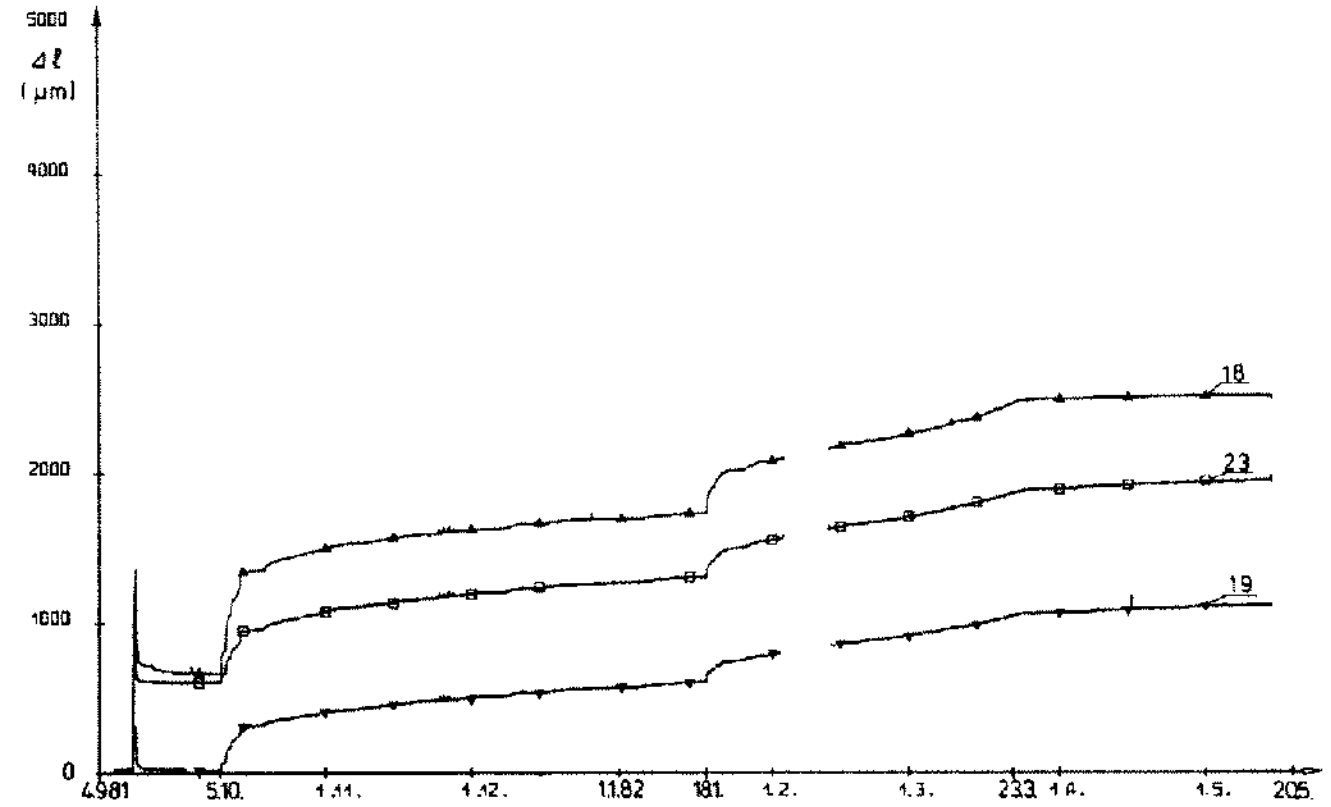

Figure 6. Deformation-time curves of three vertical measuring intervals. Measuring interval 0.5 m. Numbers indicate numbers of measuring intervals.

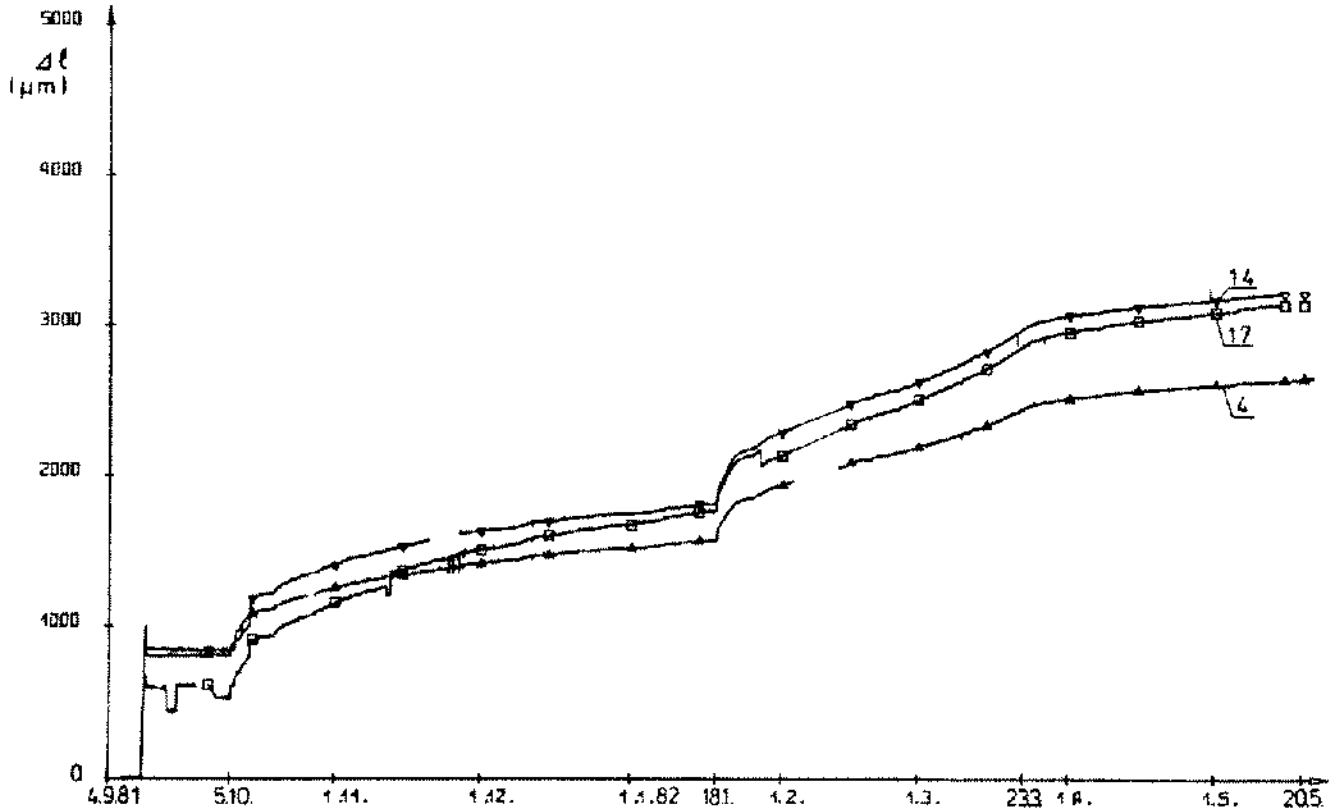

Figure 7. Deformation-time curves of the three horizontal measuring intervals. Measuring interval 1 m. Numbers indicate numbers of measuring intervals.

TABLE 1

Mean Values of the Displacements During Different Periods

		05.10.81–18.01.82	18.01.82–14.05.82	05.10.81–14.05.82
Vertical compression	upper part	1.39 mm	0.90 mm	2.29 mm
	lower part	1.25 mm	0.97 mm	2.23 mm
	total	2.64 mm	1.87 mm	4.52 mm
Extension of flatjack		3.15 mm	1.75 mm	4.90 mm
Horizontal extension		0.97 mm	1.28 mm	2.25 mm

which took place, the displacements of the 1-m-long measuring lengths are summarized in Table 1 for several periods of time. The total strain in both pillar halves was roughly 1.5 times the total compression given in Table 1. The total measuring length was 2 m; however, the pillar height was 3 m. If one follows this calculation through, then one notices that the flatjack expansion in all cases is a little less than the total compression of the two pillar halves. This indicates a small amount of convergence of the drift, which does in fact emerge from the results of the extensometer measurements (see Figure 13).

Even more important for further investigation is the statement of the strain rates in both phases of steady-state creep, at 9.3 and 10.33 MPa. Mean values are given here for the 1-m-long vertical and horizontal measuring intervals, as well as for the 0.5-m-long vertical intervals. For the vertical, 0.5-m-long measuring intervals, it is necessary to differentiate between that bordering the flatjack (= inside) and that bordering the floor or roof (= outside) (see also Figure 1). The data obtained are compared in Table 2 with the values obtained from the BGR creep law. The creep rates of the vertical measuring intervals are graphically compared with the creep law as seen in Figure 8.

It can be seen that the measured creep rates are somewhat lower than those calculated in accordance with the formula.

As mentioned above, supplementary laboratory tests for creep behaviour were carried out on 10 selected samples from the test pillar. In this case, 6 cube-shaped samples with an edge length of 75 mm were tested, as well as 4 cylindrical samples with a length of 211.4 mm and a diameter of 84.6 mm. The results for the steady-state creep rates of the individual samples can be seen in Tables 3 and 4.

The values for the cube-shaped and cylindrical samples show only slight scattering, despite the difficult measurements involved with these low stresses. The average creep rates are plotted in Figures 9 and 10, together with the curve of the BGR creep law.

The laboratory tests show that the behaviour of the cube-shaped samples is slightly different from that of the cylindrical samples. With one exception, in spite of end-face lubrication, the cube-shaped samples deformed more slowly than did the cylindrical samples. However, the results all fall within the scope of the BGR creep law.

The most important aim of the in situ test was to compare the creep rates determined in a large salt pillar with those determined in the laboratory test and those from the BGR creep law. In summarizing, it can be said that the average steady-state creep rates of the vertical measuring intervals on the salt pillar halves are somewhat smaller than those calculated. This behaviour is also shown for the cube-shaped samples in laboratory tests, at least with the greater stresses. Overall, with respect to steady-state creep, there was good agreement in the creep behaviour of the cube-shaped laboratory samples and those of the in situ salt pillar.

A further detailed evaluation concerning the deformation behaviour of the pillar and the surrounding rock is presented below in comparison with the finite element computation. This comparison confirms the statement made above.

The results of the extensometer measurements, the accuracy of which is within 0.1 mm, are shown in Figures

TABLE 2

Average Steady-State Creep Rates $\dot{\epsilon}_s(d^{-1})$ in the Salt Pillar

	σ = 9.3 MPa		σ = 10.33 MPa	
Measuring Interval	**Measured**	**Calculated**	**Measured**	**Calculated**
1 m vertical	2.50×10^{-6}	5.6×10^{-6}	6.46×10^{-6}	9.5×10^{-6}
0.5 m vertical (outside)	3.35×10^{-6}	5.6×10^{-6}	7.61×10^{-6}	9.5×10^{-6}
0.5 m vertical (inside)	2.33×10^{-6}	5.6×10^{-6}	5.71×10^{-6}	9.5×10^{-6}
1 m horizontal	4.03×10^{-6}	2.8×10^{-6}	9.58×10^{-6}	4.8×10^{-6}

Temperature T = 28.5°C. The calculated creep rates are derived from the BGR creep law.

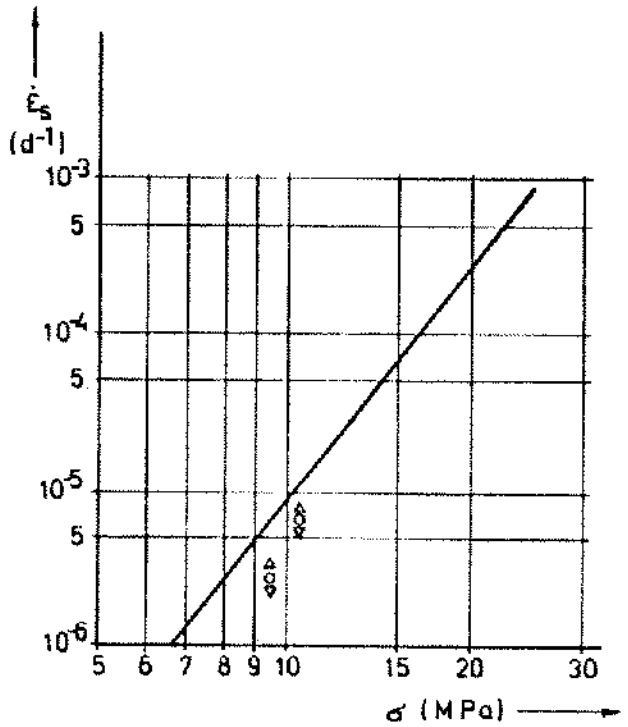

Figure 8. Representation of the mean steady-state creep rates in the vertical direction from Table 2, in relation to the stress. The straight line represents the BGR creep law for T = 28.5°C. Measuring intervals: ○: 1 m vertical, △: 0.5 m vertical (outside), ▽: 0.5 m vertical (inside).

11-14. The displacements of the lengths, F9, S9, B and G (see Figure 3) are plotted as functions of time, in each case the mean values for the 4 pillar sides. F9 and S9 show an overall lengthening, whereas length B becomes shorter. This indicates a convergance of the cavity. The overall length G shows a shortening.

TABLE 3

Steady-State Creep Rates $\dot{\varepsilon}_s$(d^{-1}) Determined from Laboratory Tests

Sample	σ = 11 MPa	σ = 15 MPa	σ = 16 MPa
Cubes			
B6-1/W	1.4×10^{-5}	2.6×10^{-5}	5.5×10^{-5}
B6-2/W	1.0×10^{-5}	2.3×10^{-5}	5.3×10^{-5}
B4-3/W	8.2×10^{-6}	2.7×10^{-5}	5.9×10^{-5}
Cylinders			
B4-2/Z	5.8×10^{-6}	5.5×10^{-5}	1.5×10^{-4}
BS-2/Z	5.8×10^{-6}	5.6×10^{-5}	1.3×10^{-4}
Average cubes	1.07×10^{-6}	2.50×10^{-5}	5.6×10^{-5}
Average cylinders	5.80×10^{-6}	5.55×10^{-5}	1.4×10^{-4}
Calculated	1.07×10^{-5}	5.02×10^{-5}	6.9×10^{-5}

Temperature T = 26°C. The calculated creep rates are derived from the BGR creep law.

TABLE 4

Steady-State Creep Rates $\dot{\varepsilon}_s$(d^{-1}) Determined from Laboratory Tests

Sample	σ = 10 MPa	σ = 14 MPa
Cubes		
B6-1/W-2	9.0×10^{-6}	1.9×10^{-5}
B6-2/W-2	9.0×10^{-6}	2.1×10^{-5}
B4-3/W-2	1.0×10^{-5}	2.3×10^{-5}
Cylinders		
B6-1/Z-2	2.7×10^{-5}	5.1×10^{-5}
B4-2/Z-2	2.7×10^{-5}	5.2×10^{-5}
Average cubes	9.3×10^{-6}	2.1×10^{-5}
Average cylinders	2.7×10^{-5}	5.2×10^{-5}
Calculated	5.0×10^{-6}	2.7×10^{-5}

Temperature T = 22°C. The calculated creep rates are derived from the BGR creep law.

NUMERICAL COMPUTATIONS

Computational investigations into in situ tests already carried out were undertaken with the aim of a better interpretation of rock mechanical measurements in their entirety, and so that the mechanical processes in rock can be more accurately analysed.

On the other hand, numerical computations should

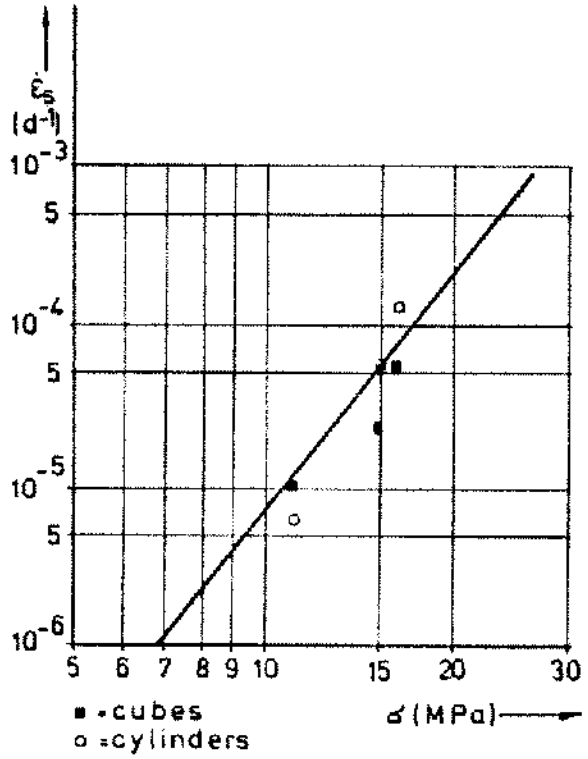

Figure 9. Representation of the mean steady-state creep rates from the laboratory tests with T = 26°C in Table 3, in relation to the stress. The straight line represents the BGR creep law.

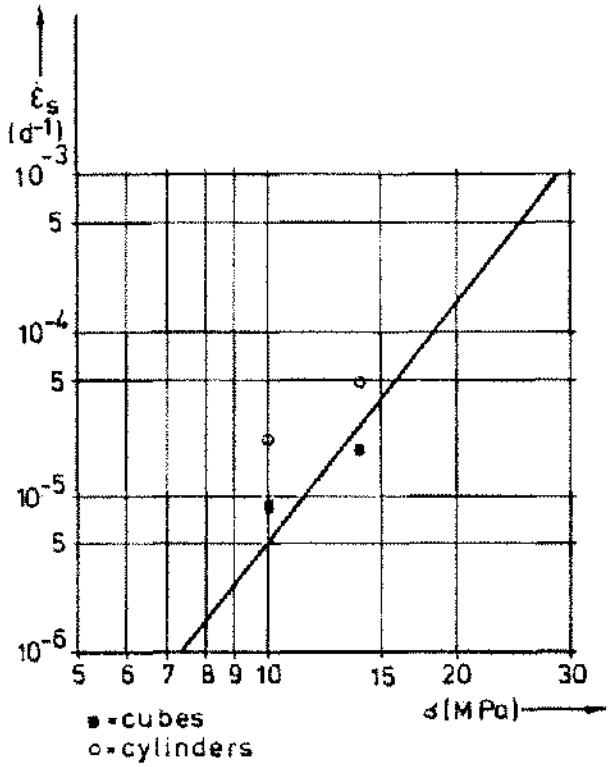

Figure 10. Representation of the mean steady-state creep rates from the laboratory tests with T = 22°C in Table 4, in relation to the stress. The straight line represents the BGR creep law.

help in the verification of constitutive relations, so that the characteristic values determined in the laboratory can be more reliably extrapolated for in situ conditions.

The model computations for the pillar test in the Asse salt mine were carried out on the finite element mesh shown in Figure 15. For reasons of symmetry, only a quarter of the whole section is shown. A geometrical idealisation results from a simplified axisymmetric model. In view of the symmetrical characteristics, the computation was limited to the upper part of the rock under consideration. The finite element mesh is composed of 131 isoparametric elements. The finite element mesh has 448 nodes.

The elastic constants on which the computation is based are E-24000 MPa and $\nu = 0.25$. In the description of the time-dependent material behaviour, only steady-state creep was considered. The assumed creep law developed in the BGR is as follows:

$$\dot{\varepsilon}^{s}_{eff} = A \cdot \exp\left(-\frac{Q}{RT}\right) \cdot \left(\frac{\delta_{eff}}{\delta^*}\right)^n$$

where

$A = 0.18\ d^{-1}$
$Q = 54\ kJ \cdot mol^{-1}$
$R = 8.3143 \cdot 10^{-3}\ kJ \cdot K^{-1} \cdot mol^{-1}$
$\delta^* = 1.0$ MPa
$n = 5.0$.

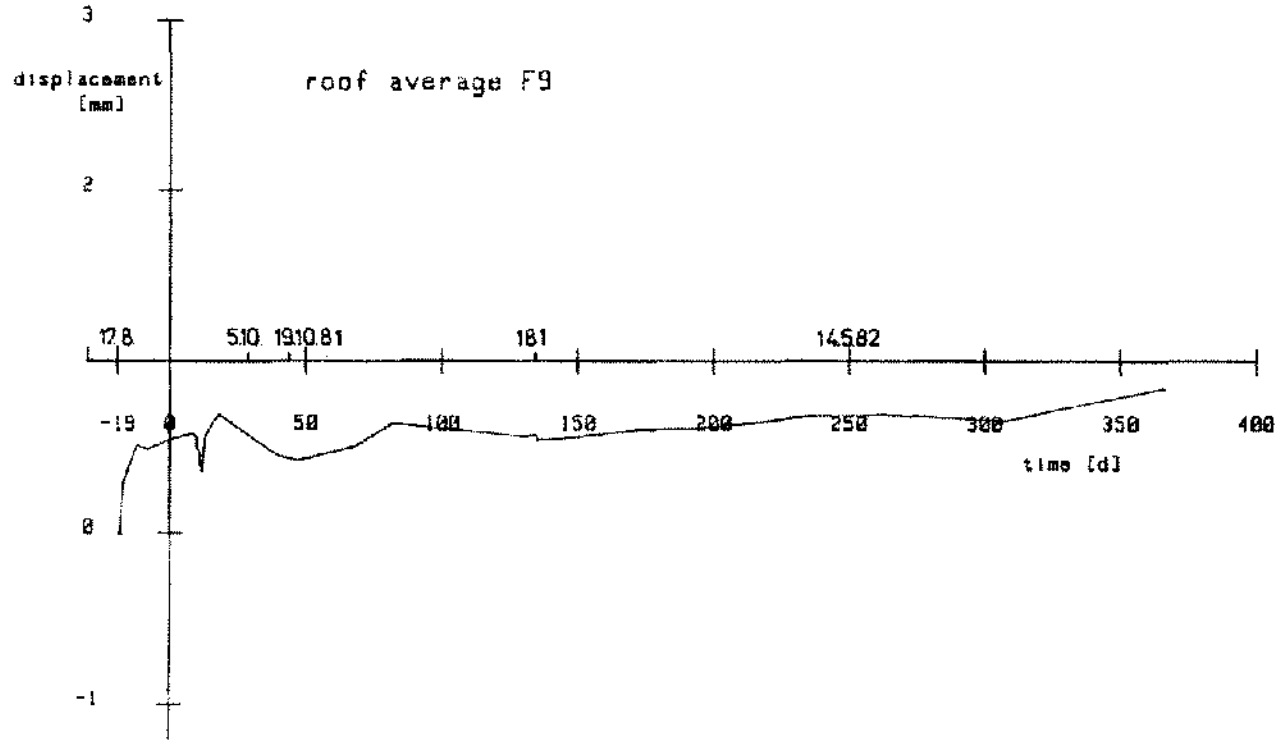

Figure 11. Deformation-time curve of extensometer measuring interval F9 (see Figure 3). This is the mean value of the four pillar sides.

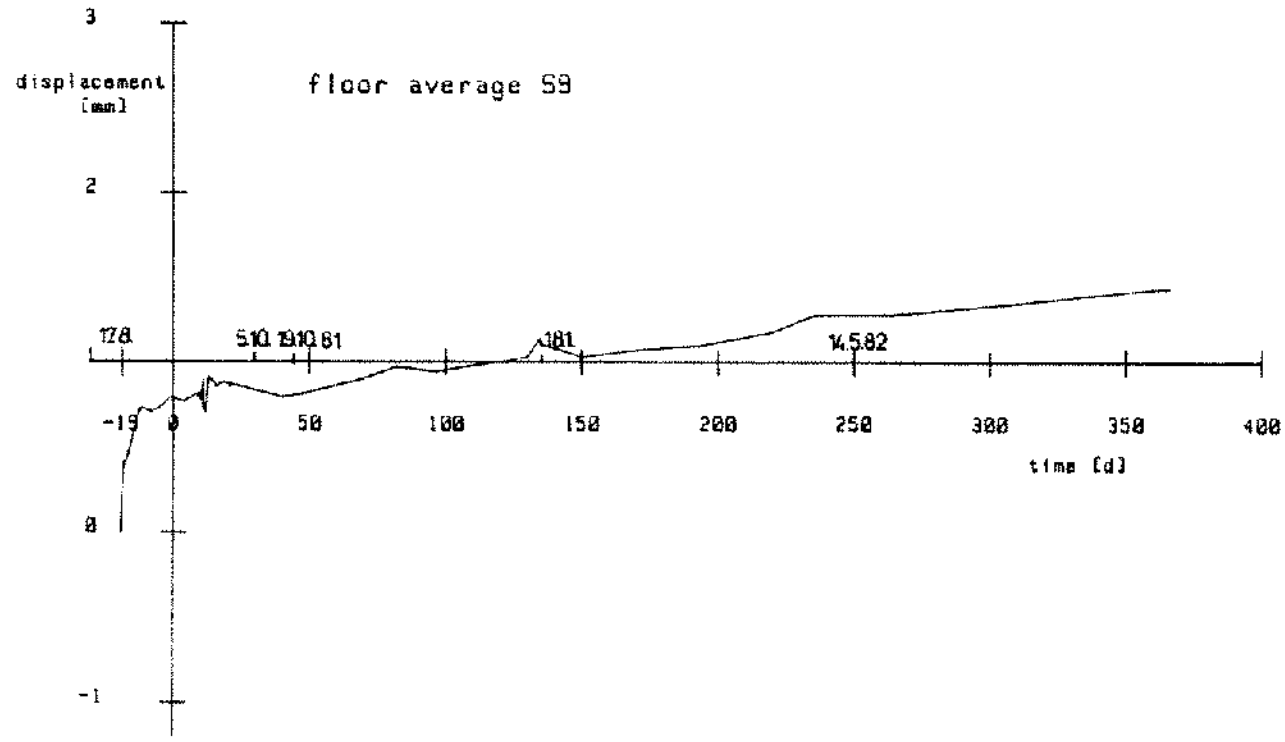

Figure 12. Deformation-time curve of extensometer measuring interval S9 (see Figure 3). This is the mean value of the four pillar sides.

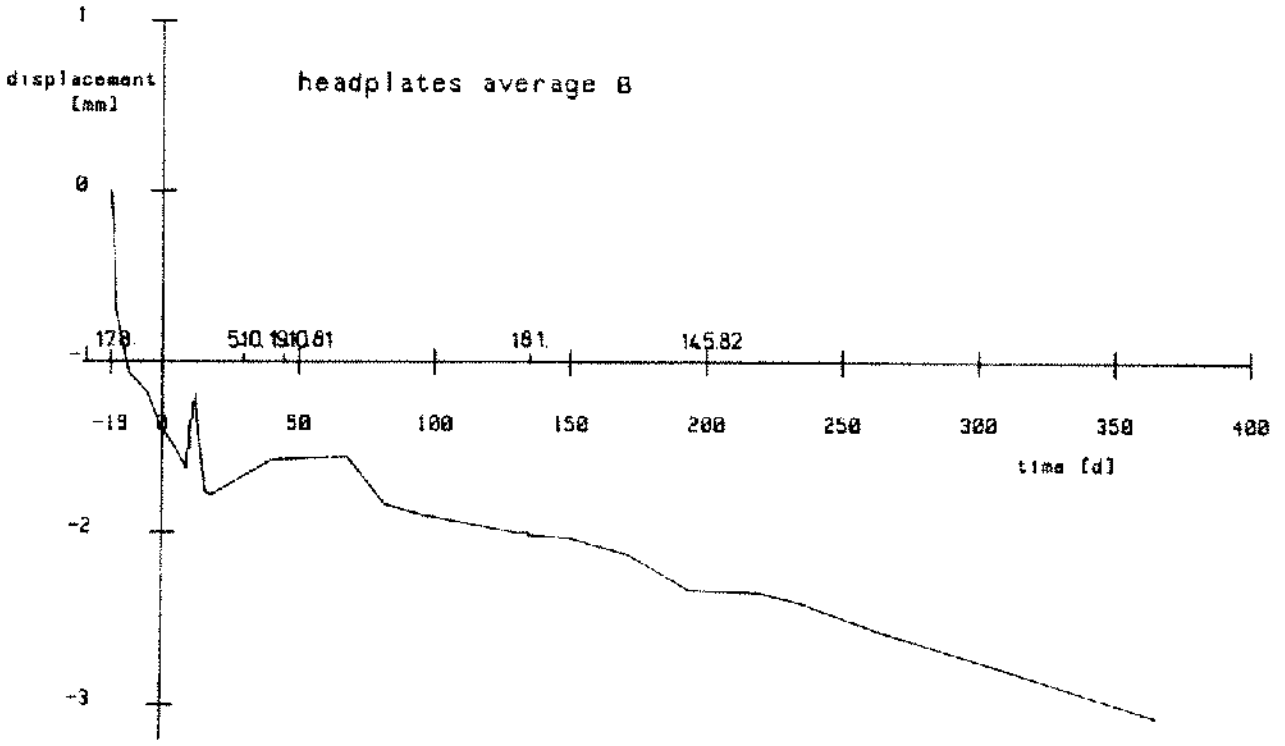

Figure 13. Deformation-time curve of extensometer measuring interval B (see Figure 3). This is the mean value of the four pillar sides.

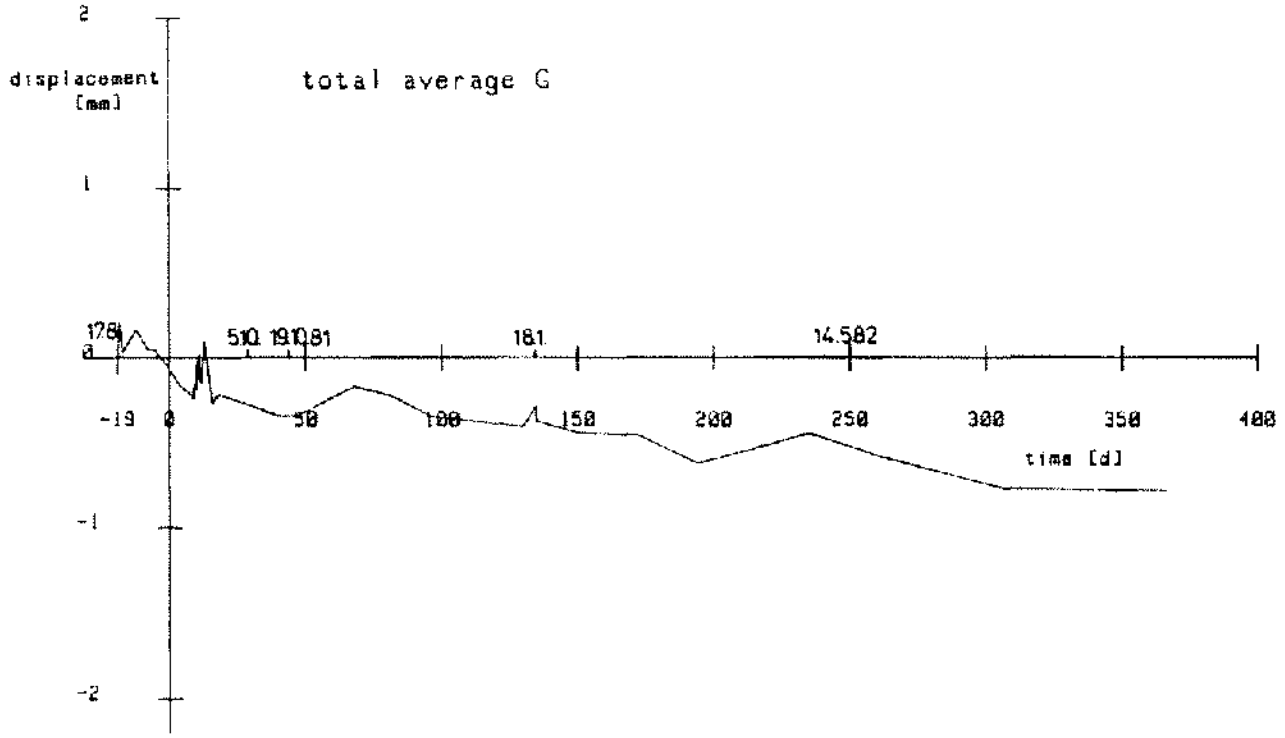

Figure 14. Deformation-time curve of extensometer measuring interval G (see Figure 3). This is the mean value of the four pillar sides.

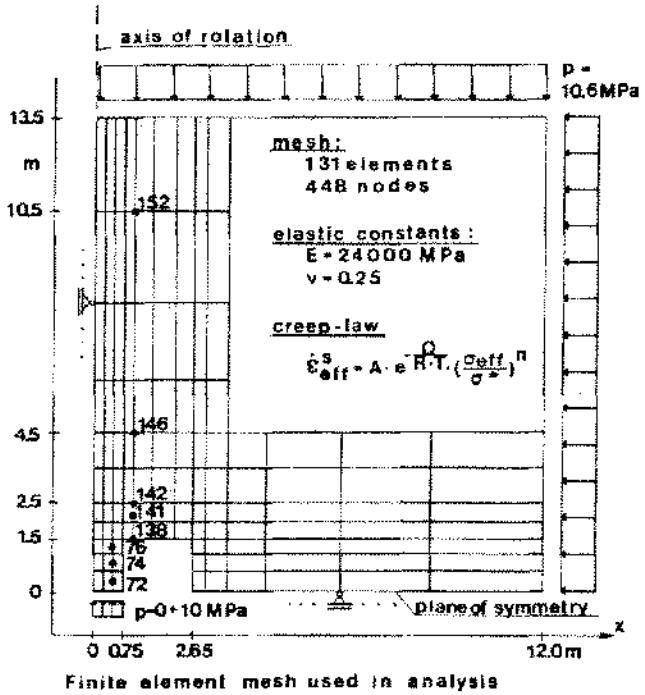

Figure 15. The axisymmetric finite element mesh used in the model calculations of the time-dependent deformation of the salt pillar and the surrounding rock. Due to the symmetry of the model, only one quarter of the cross-section is shown. The displacements of the numbered nodes are described in the text.

A hydrostatic initial state of stress of $\delta r = \delta p = 10.6$ MPa, which corresponds to the petrostatic pressure, was assumed for computation of the initial elastic results at time $t = 0$.

The distribution of the principle stresses as shown in Figure 16 illustrates the supporting behaviour in the vicinity of the pillar. The representation given here is an example for time $t = 0$.

In the model caculation the excavation of the room around the pillar occurs at time $t = 0$, followed by a creep phase of 49 days until the cutting of the slit. In this period the vertical stress in the pillar is greatly reduced. This and the further vertical stress history immediately above the flatjack are shown in Figure 17. When comparing the curves resulting from the model computation with the measured curves, it should be noted that the time 0 points do not agree, as the measurements in the in situ test were started with the cutting of the slit. The calculation began with 1 July 1981, the time scale of the measurement curves on 4 Sept. 1981, i.e., 66 days later. The vertical displacement histories of the three finite element mesh node points 72, 74 and 76, distributed from the bottom to the top of the pillar, are shown in Figure 18. Here, in the 14-day loading phase it can be seen that the pillar halves are forced strongly upward or downward. In the following phase, in which the pressure in the

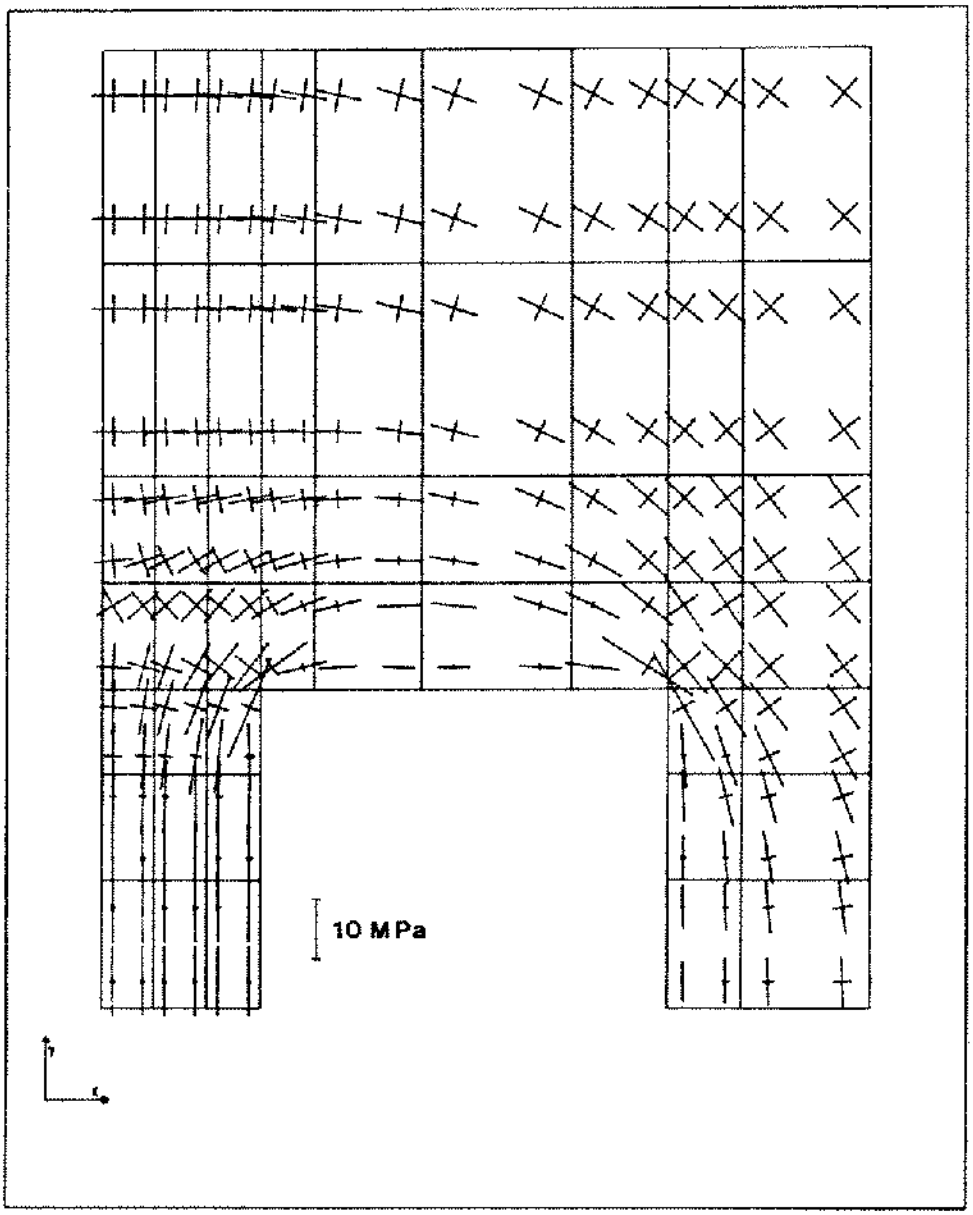

Figure 16. The calculated distribution of the principle stresses in the pillar and in the surrounding rock immediately after construction of the pillar at time t = 0.

flatjack is kept constant, this process slows considerably in the central pillar area. Near the top of the pillar, the direction of movement is even reversed. Point 76 moves downward because of the existing rock pressure.

The horizontal displacement history of these three points is plotted in Figure 19. Moreover, the curves for points 72 and 74 clearly show that the displacements seen over the length of the pillar have almost the same value. Only at the top (Point 76) is there a smaller horizontal displacement of the pillar due to the clamping effect of the surrounding rock.

This constraint is clearly illustrated by Figures 20 and 21, which show the deformed structure of the pillar immediately before the application of pressure in the flatjack, as well as after 280 days. The removal of stress from the pillar due to cutting of the slit can be clearly seen in Figure 20, whereas the compression of the pillar due to loading in Figure 21. In both figures, the vertical displacement of the rock above the pillar results mainly from the excavation phase, as well as from the cutting of the slit.

In view of the clamping effect of the rock in the horizontal direction, the almost uniaxial state of stress in the pillar top is disturbed, as the distribution of the principal stresses for t = 280 days shows in Figure 22.

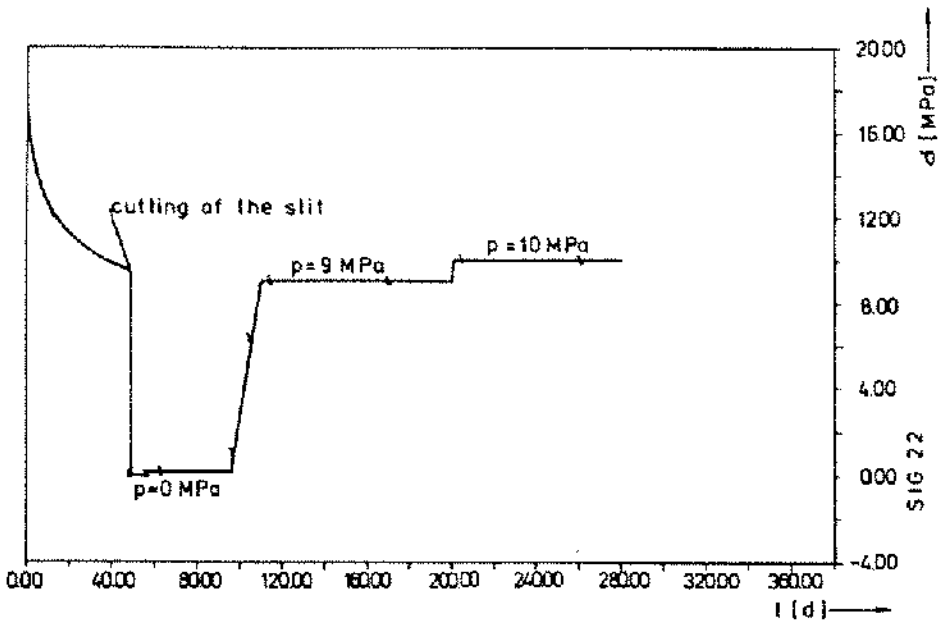

Figure 17. The calculated chronological development of the vertical stress immediately above the flatjack, from construction of the pillar onwards.

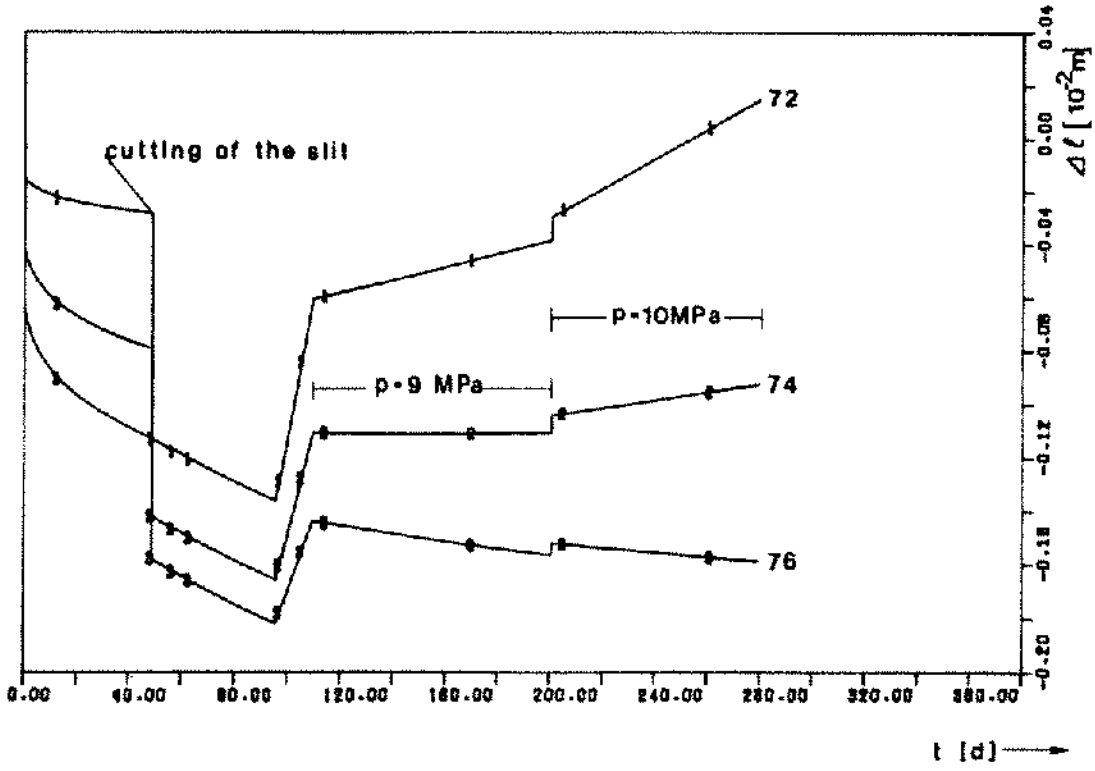

Figure 18. Computed vertical displacements of node points 72, 74 and 76 of the finite element mesh, relative to the horizontal plane of symmetry.

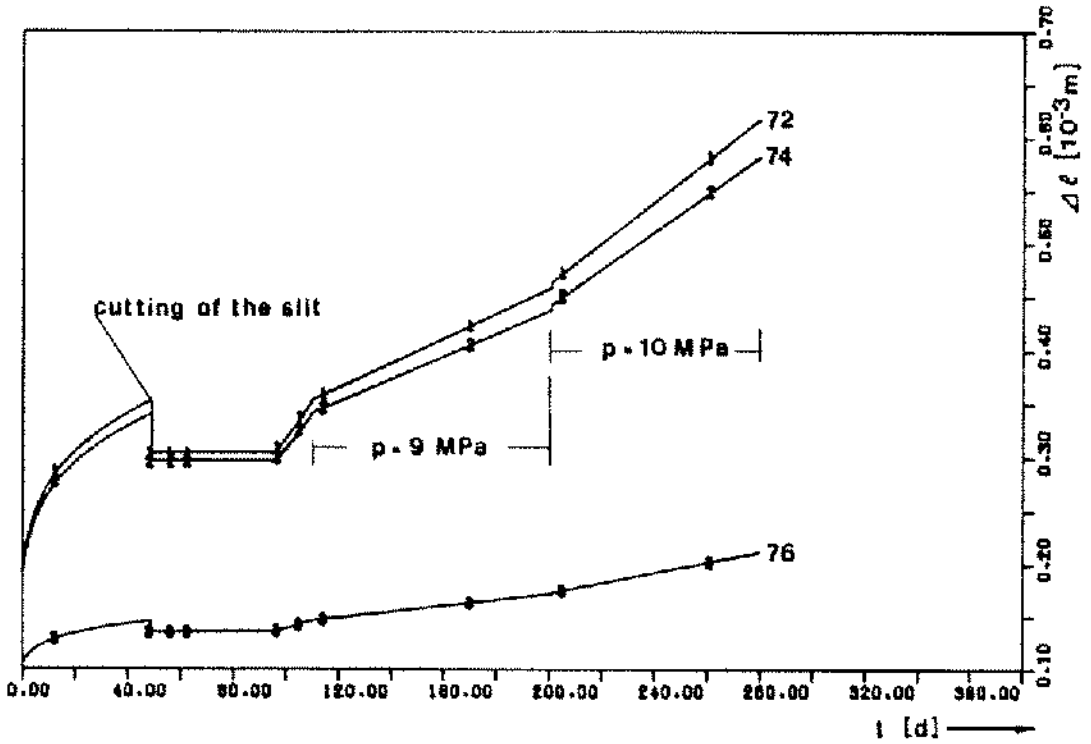

Figure 19. Computed horizontal displacements of node points 72, 74 and 76 of the finite element mesh, relative to the vertical axis of rotation. Note that the scale differs from that in Figure 18.

TABLE 5

Comparison of Measured and Computed Creep Rates in the Test Pillar, in the Vertical Direction

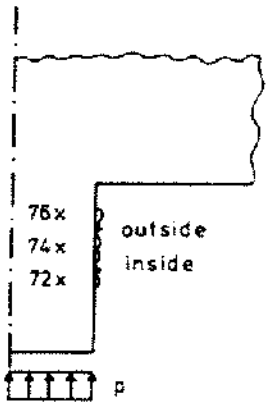

Measuring Interval	Pressure in Flatjack	Steady State Creep Rate $\dot{\epsilon}_s(d^{-1})$ Derived From:		
		Model Calculation	Measurement	Theory
72–76	9 MPa	3.83×10^{-6}	2.50×10^{-6}	4.25×10^{-6}
72–74	9 MPa	4.40×10^{-6}	2.33×10^{-6}	4.25×10^{-6}
74–76	9 MPa	3.12×10^{-6}	3.35×10^{-6}	4.25×10^{-6}
72–76	10 MPa	6.43×10^{-6}	6.46×10^{-6}	7.2×10^{-6}
72–74	10 MPa	7.42×10^{-6}	5.71×10^{-6}	7.2×10^{-6}
74–76	10 MPa	5.22×10^{-6}	7.61×10^{-6}	7.2×10^{-6}

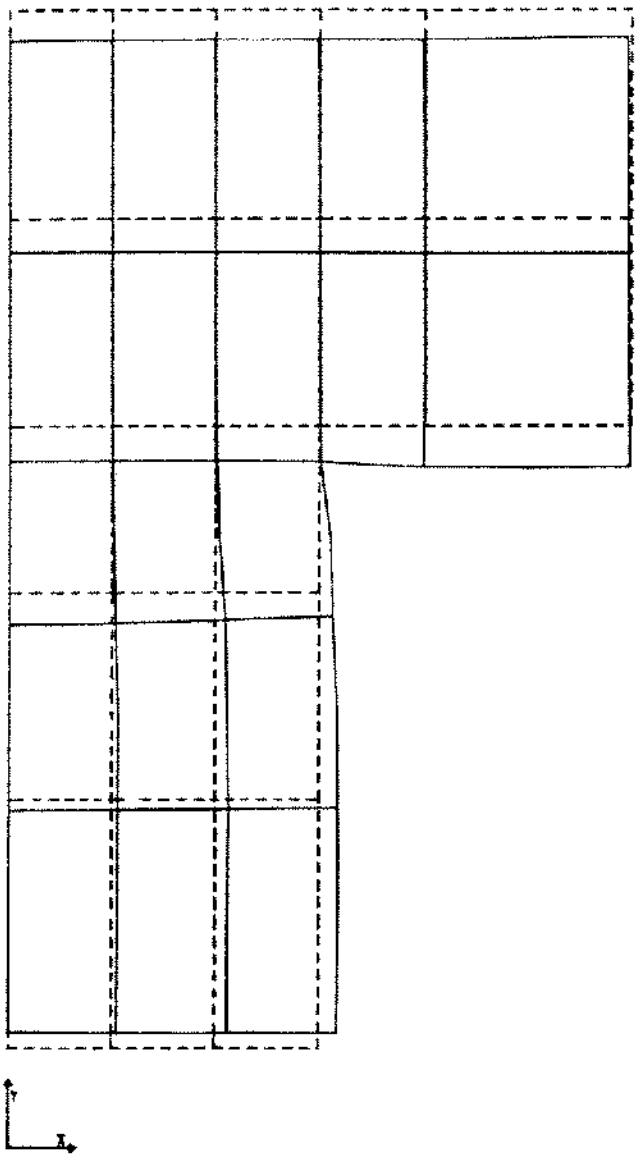

Figure 20. Representation of the computed deformation of the pillar and its immediate surroundings at time t = 96 days, immediately before application of pressure. The Figure shows a section of the finite element mesh. ---- Undeformed finite element mesh., —— Deformed finite element mesh., The deformations are represented with ×50 exaggeration.

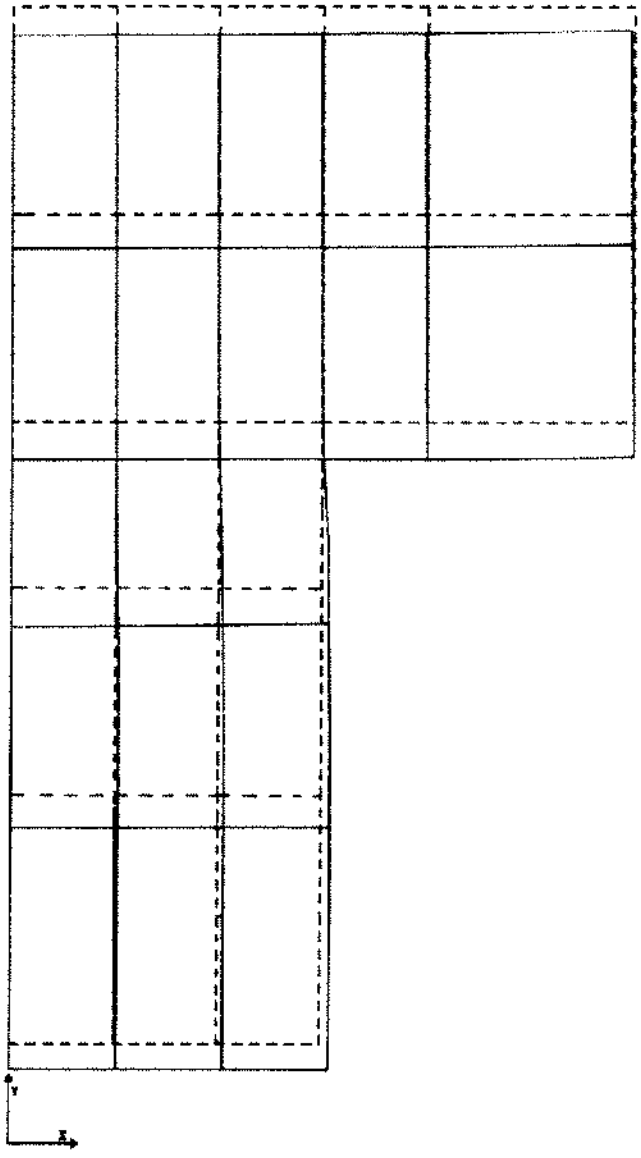

Figure 21. Representation of the computed deformation of the pillar and its immediate surroundings at point of time t = 280 days. The figure shows a section of the finite element mesh. ---- Undeformed finite element mesh. —— Deformed finite element mesh. The deformations are represented with ×50 exaggeration.

The influence of the in situ test on the deformation behaviour of the surrounding rock can be seen from Figure 23. It shows the vertical displacement history of the multi-extensometer measuring points at distances of 0.75, 1.0, 3.0 and 9.0 m from the head plate. In general, deformation behaviour is the same as at the top of the pillar (see Figure 18). With increasing distance from the excavation, however, the influence of the in situ test is significantly reduced. The effects at a depth of 9 m are only of a minor nature.

COMPARISON OF RESULTS FROM COMPUTATION AND MEASUREMENT

In this section, deformation measured on the pillar and in its vicinity during the in situ creep test are compared with the results of the finite element model computations. In addition, creep rates calculated from the BGR creep law for the case of the ideal uniaxial state of stress are given in Tables 5 and 6 and marked with the word "theory."

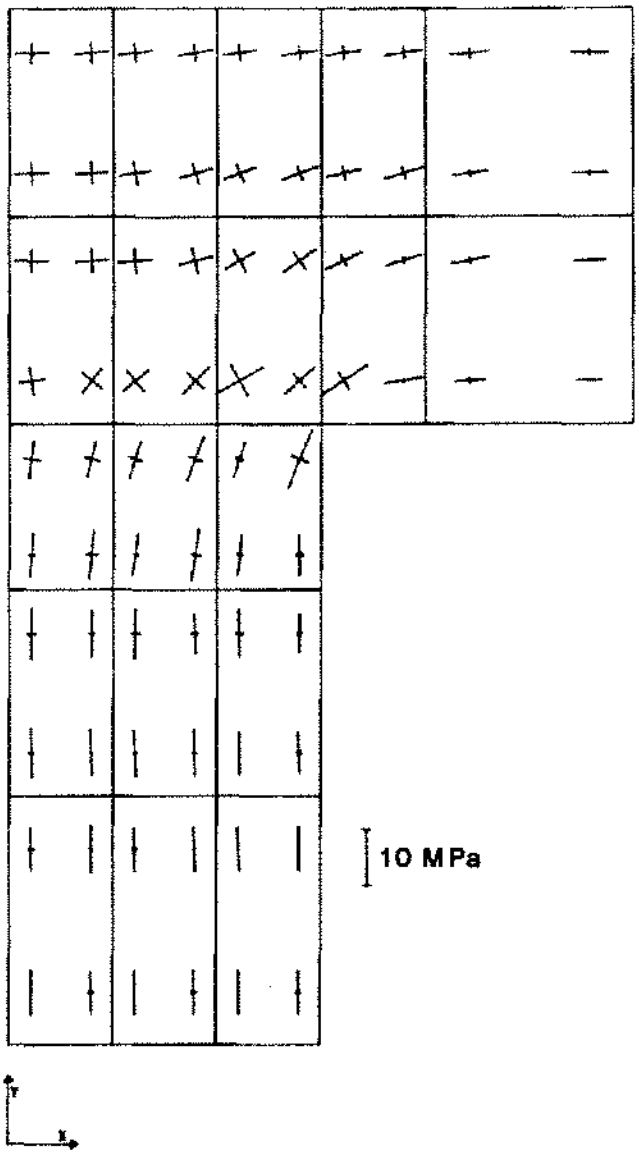

Figure 22. The computed distribution of principle stresses in the pillar and in its immediate surroundings at time t = 280 days.

In Table 5, the three steady-state creep rates determined in the vertical direction are given for two pressure stages and for various intervals on the pillar halves in Table 5. For the 1-m-long interval (72–76), the results of the measurement and computation are largely in agreement. As already established, the theoretical values always lie above those measured, in both pressure stages.

A study of the results for the 0.5-m-long measurement interval also reveals a satisfactory agreement between the model computation and measurement. There is, however, one discrepancy. According to the results of the model computation, the outer part of the pillar (74–76) creeps more slowly than the inner part (72–74) due to the clamping effects of the rock. According to the measurements, the reverse is the case. An explanation for this difference has not yet been found.

The comparison of the horizontal creep rates is summarized in Table 6. In theory, assuming incompressibility, a horizontal creep rate is determined in accordance with the creep law that is only half as great as that in the vertical direction. Near the slit (A-72 and A-74), the creep rates from "theory" and model computations are in good agreement; farther from the slit, at the top of the pillar (A-76), the model computation clearly shows the clamping effect of the surrounding rock. The measurements from the in situ experiment show, however, that the horizontal creep rate is even greater than the creep rate in the vertical direction. This indicates an increase in volume of the pillar.

Two computations were carried out using different distances between the pillar and the surrounding salt-rock in order to determine the influence of these lengths on the deformations in the surrounding rock. As expected, the results showed no difference in the creep behaviour of the pillar. The differing support spans do have a significant effect on the convergence of the rock, as is clearly shown in Table 7. It shows the mean deformation-velocities of the head plate in the roof during the two loading phases, as determined from both model computations and the in situ measurement. The observed results show a large measure of agreement with both computed results. A further evaluation of the extensometer measurements is not undertaken within the scope of this study, as investigations into the pillar creep rate were of prime importance.

Overall, it can be stated that the agreement between measurement and model computation is quite good in almost all points. It must also be stressed that the computations were not repeated to obtain closer agreement with the measurements. The agreement between the comprehensive measurements and the model computations, the input data of which were supported by laboratory tests, reconfirm that large rock salt masses are deformed according to the same laws as laboratory samples.

ACKNOWLEDGMENTS

The in situ test and the investigations into the reference samples were carried out within the scope of SR 138 project "Rock Mechanics in Salt," sponsored by the BMI as well as project KWA 5202/6 "Deformation mechanisms," sponsored by the BMFT. The computations were carried out using the program system ANSALT within the scope of research project KWA 5203/7 "Comparison of thermomechanical computations with thermomechanical in situ tests."

Grateful thanks are expressed to Dr. Wallner (BGR) for his assistance and support during the finite element computations.

At this point we wish to extend our thanks to the staff of the IfT (Institut für Tieflagerung) of GSF (Gesellschaft für Strahlen-und Umweltforschung) for construction of the pillar, extensometer measurements and data recording.

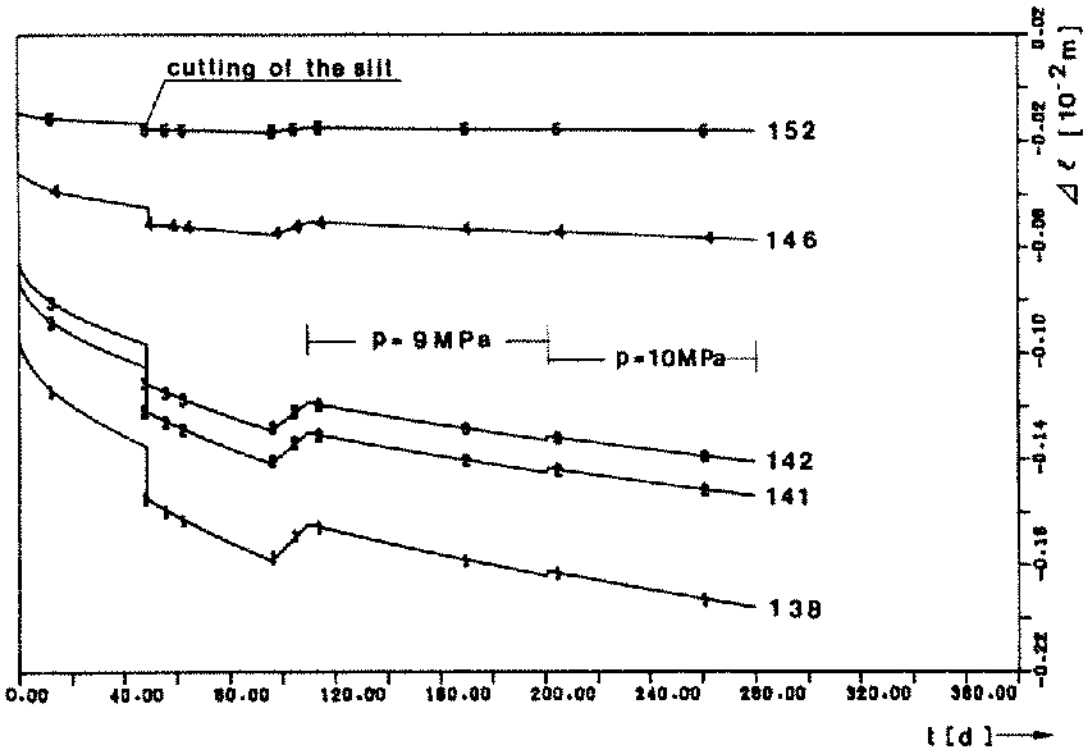

Figure 23. Computed vertical displacements of the extensometer points in Figure 3 and Figure 15, in relation to the horizontal plane of symmetry.

TABLE 6

Comparison of Measured and Computed Creep Rates in the Test Pillar, in the Horizontal Direction

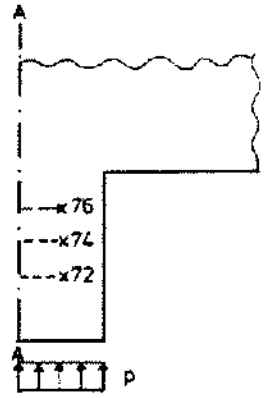

Measuring Interval	Pressure in Flatjack	Steady State Creep Rate $\dot{\epsilon}_s[d^{-1}]$ Derived From:		
		Model Calculation	Measurement	Theory
A-76	9 MPa	0.56×10^{-6}	—	2.13×10^{-6}
A-74	9 MPa	2.1×10^{-6}	4.0×10^{-6}	2.13×10^{-6}
A-72	9 MPa	2.3×10^{-6}	—	2.13×10^{-6}
A-76	10 MPa	0.97×10^{-6}	—	3.6×10^{-6}
A-74	10 MPa	3.5×10^{-6}	9.6×10^{-6}	3.6×10^{-6}
A-72	10 MPa	3.9×10^{-6}	—	3.6×10^{-6}

TABLE 7

Summary of the Mean Deformation Velocities of the Extensometer Head Plates in Relation to the Horizontal Plane of Symmetry

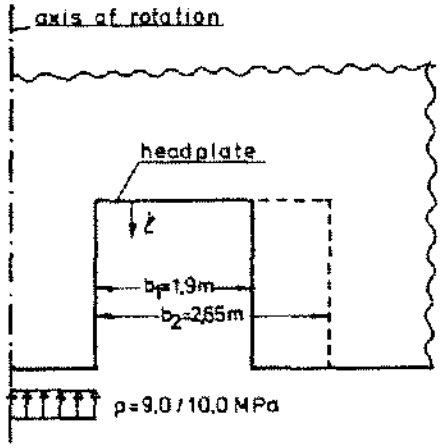

phase of load
p_1 = 9 MPa t = 110-201 d
p_2 = 10 MPa t = 201-280 d

Pressure in Flatjack	Deformation Velocity 1 (mm/d) Derived From: Calculation 1 b = 1.9 m	Calculation 2 b = 2.65 m	Measurement
9 MPa	2.18×10^{-3}	3.21×10^{-3}	2.9×10^{-3}
10 MPa	1.76×10^{-3}	2.65×10^{-3}	1.8×10^{-3}

The values derived from two finite element computations with different spans (b_1 and b_2) are given, as well as those from the measurements of the in situ test for two loading stages.

REFERENCES

Albrecht, H. and U. Hunsche. 1980. Gebirgsmechanische Aspekte bei der Endlagerung radioaktiver Abfälle in Salzdiapiren unter besonderer Berücksichtigung des Fliessverhaltens von Steinsalz. Fortschr. Miner. V. 58(2):212-247.

Ashby, M.F. 1972. A first report on deformation mechanism maps. Acta Met. V. 20:887-897.

Dreyer, W. 1972. The science of rock mechanics. Part 1. The strength properties of rocks. Trans. Tech. Publications, Bay Village, Clausthal—Zellerfeld.

Frost, H. J. 1974. Deformation mechanism maps. Ph.D. Thesis, 302 pp., Harvard Univ., Cambridge, Mass.

Herrmann, W., W. R. Wawersik and H. S. Lauson. 1980. Analysis of steady state creep of Southeastern New Mexico bedded salt. Sandia National Laboratories, Albuquerque NM, SAND-80-0558, 43 pp.

Hunsche, U. 1982. Results and interpretation of creep experiments on rock salt. Proc. First Conf. on the Mechanical Behavior of Salt, 9-11 Nov. 1981, The Penn. State Univ., University Park, Pa.

Langdon, T. G. 1978. Recent developments in deformation mechanism maps. Metals Forum V. 1:59-70.

Tsur-Lavie, Y. and S. A. Denekamp. 1982. Comparison of size effect for different types of strength tests. Rock Mech. V. 15:243-254.

Wallner, M., C. Caninenberg and H. Gonther. 1979. Ermittlung zeit- und temperaturabhängiger mechanischer Kennwerte von Salzgesteinen. Proc. 4. Int. Congr. Rock Mech., Montreux 1979, V. 1:313-318.